Annales
Geophysicae

The polar cliff in the morning sector of the ionosphere

G. W. Prölss

Argelander Institut für Astronomie, Universität Bonn, Auf dem Hügel 71, 53121 Bonn, Germany

Correspondence to: G. W. Prölss (gproelss@astro.uni-bonn.de)

Abstract. By "polar cliff" we mean the steep increase in the ionization density observed in the morning sector of the polar ionosphere. Here the properties of this remarkable feature are investigated. The data set consists of electron density and temperature measurements obtained by the Dynamics Explorer 2 satellite. Only data recorded in the Northern Hemisphere winter are considered (solar zenith angle $\geq 90°$). We find that for moderately disturbed conditions, the foot of the polar cliff is located below $60°$ invariant latitude. Here, within about $4°$, the density increases by a factor of 4, on average. The actual location of the polar cliff depends primarily on the level of geomagnetic activity, its associated density increase on geographic longitude and altitude. As to the longitudinal variations, they are attributed to asymmetries in the background ionization density at middle latitudes. Using a superposed epoch type of averaging procedure, mean latitudinal profiles of the polar cliff and the associated electron temperature changes are derived. Since these differ significantly from those derived for the afternoon/evening sector, we conclude that the subauroral ionospheric trough does not extend into the morning sector. As to the origin of the polar cliff in the morning sector, local auroral particle precipitation should play only a secondary role.

Keywords. Ionosphere (Polar ionosphere)

1 Introduction

The most striking phenomenon observed in the morning sector of the ionosphere at higher latitudes is a steep – sometimes step-like – increase in the ionization density; see Fig. 1. For convenience of reference, this feature will be called "polar cliff". Although discovered almost 50 yr ago (e.g., Liszka, 1965; Thomas et al., 1966), little is known about this remarkable phenomenon (e.g., Andrews and Thomas, 1969; Taylor, 1973; Dudeney et al., 1983; Rodger et al., 1986; Middleton

et al., 2008; Rodger, 2008). In fact, its mean properties have never been determined! Here an attempt is made to fill this gap.

The general format of our presentation resembles that of previous studies by the author on related polar phenomena (Prölss, 2006a,b, 2007, 2008). First, the data selection and processing are described (Sect. 2). Next, the location of the polar cliff and its dependence on various geophysical parameters is determined (Sect. 3). In a similar way, the magnitude of the density rise is investigated (Sect. 4). In Sect. 5, the mean latitudinal profiles of the polar cliff and the associated electron temperature changes are derived. It follows a discussion of our results and a comparison with related observations (Sect. 6). Finally, the main findings of our study are summarized in Sect. 7.

2 Data selection and processing

We again use the electron density and temperature measurements obtained by the Langmuir probe aboard the Dynamics Explorer 2 satellite. A general description of this satellite is given in Hoffman and Schmerling (1981), and details on the Langmuir probe experiment can be found in Krehbiel et al. (1981). Here the data contained in the unified abstract file prepared by the NASA National Space Science Data Center are analyzed.

In the present study, only data obtained in the Northern Hemisphere are considered. This facilitates the identification of longitudinal variations which differ in both hemispheres. Second, only data obtained during winter conditions and for solar zenith angles equal or greater than $90°$ are selected. This is because magnetospherically controlled phenomena – like the polar cliff – stand out most clearly if they are not superimposed by solar radiation effects. Third, only data collected below 700 km altitude are retained because we are only interested in ionospheric phenomena. Finally – and

Fig. 1. Examples of well-defined polar cliff structures. A sequence of seven latitudinal profiles of the electron density is shown. It was obtained by the Dynamics Explorer 2 satellite on 22 December 1981. The respective universal time of observation is indicated to the left of each profile. The density is plotted on a logarithmic scale, an example of which is shown in the bottom part of the figure. For each profile, a dotted line marks the $2.3 \times 10^{10} \, \text{m}^{-3}$ density level. The data refer to the Northern Hemisphere winter. Solar local time of observation was approximately 04:40, and the magnetic local time varied between about 3 and 5 h. Typical observation heights are indicated at the top of the figure. The geomagnetic activity was relatively weak, with the AE6 index varying between 71 and 128 nT. For each profile, vertical blue lines mark the foot of the polar cliff (latf), and the first maximum/plateau (latm).

most importantly – only data obtained in the morning sector (03:00 to 09:00 magnetic local time, MLT) are considered. It is in this local time sector that the polar cliff stands out most clearly.

For each of the remaining satellite passes, the electron density was plotted as function of invariant latitude. These plots were then used to parameterize the polar cliff by visual inspection. First, the latitude (latf) of the foot of the polar cliff was determined, see Fig. 1. The associated density value is denoted as Nef. Second, the latitude (latm) of the first and most equatorward located maximum (or plateau) was determined. The associated density value is denoted as Nem. It is clear that latf can be determined with higher precision than latm. This is especially true if the density increases more gradually. In this case, the location of latm can be estimated only to within a few degrees. We also note that such a visual identification of cliff parameters always involves some subjective judgement, especially if the cliff signatures are not well defined. It is hoped, however, that our larger data sample will smooth out such deficiencies.
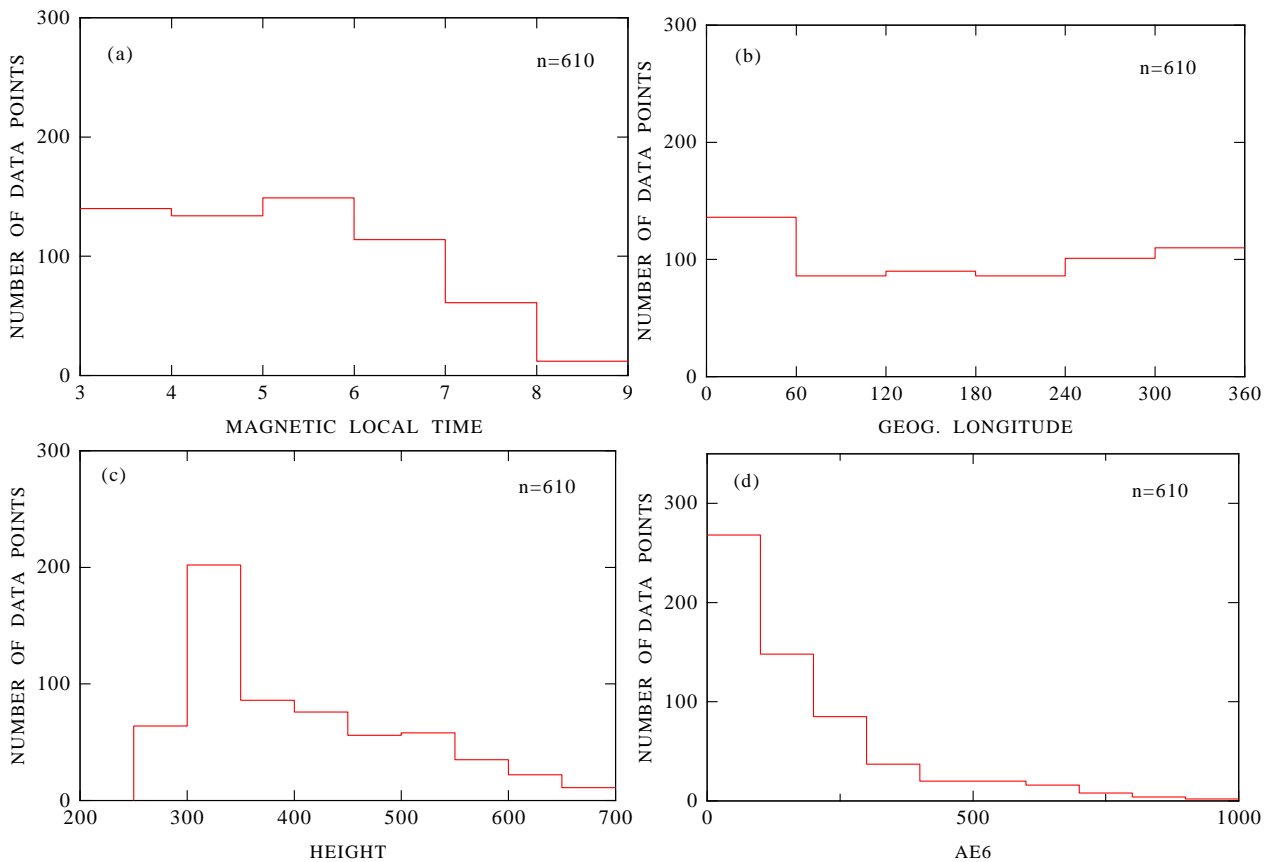
Not all density profiles allow such a parameterization. There are cases when no clear cliff structures are discernable; or when the polar cliff cannot be reliably identified in a strongly fluctuating electron density. This, however, happens in less than 6 % of all cases. Usually, all four parameters can be determined with sufficient accuracy. Altogether, 610 latitudinal profiles and their associated parameter sets are available for our analysis.

The statistics of our data set are presented in Fig. 2. As can be seen, the local time distribution is all but even, and only few data sets are available for the 08:00 to 09:00 MLT sector; see Fig. 2a. Evidently, solar radiation effects increasingly dominate the ionospheric behavior at these later morning hours. In contrast, the longitudinal distribution presented in Fig. 2b is fairly even. As to the height distribution, most data were collected in the 300 to 350 km altitude range (Fig. 2c). Finally, most data refer to weakly disturbed conditions, and only few data sets are available at activity levels above, say, AE6 = 700 nT; see Fig. 2d.

3 Location of the polar cliff

The location of the polar cliff depends primarily on the level of geomagnetic activity, to a much lesser degree on longitude and local time. Here we describe and model these variations.

The latitudes of the equatorward boundary latf and first maximum latm serve as convenient parameters to specify the location of the polar cliff. Selecting a suitable index to specify the level of geomagnetic activity is less simple, and various indices were tested. The best correlation (i.e., the highest correlation coefficient for scatter plots) was obtained for the AE6 (auroral electrojet) index introduced by Werner and Prölss (1997). This index is defined as the weighted mean of hourly averaged AE indices:

Fig. 2. Statistics of the data set analyzed in the present study. **(a)** Histogram indicating the magnetic local time distribution of the 610 electron density profiles parameterized. The time is given in hours. **(b)** Histogram indicating the geographic longitude distribution of the data set. The longitude is given in degrees east. **(c)** Histogram indicating the height distribution of the data set. The height is given in kilometers. **(d)** Histogram indicating the magnetic activity distribution of the data set. As a measure of this activity we use the AE6 index defined in Eq. (1). The units of this index are nT.

$$AE6 = \frac{\sum_{i=0}^{6} AE(UT - i[h]) e^{-i}}{\sum_{i=0}^{6} e^{-i}}. \tag{1}$$

Here UT refers to the universal time for which the AE6 index is to be calculated (in our case the universal time of the polar cliff observation). By not only considering the actual AE index but also the AE indices of the previous 6 h, this index takes the "memory effect" of the ionosphere into account. As a rough reference, we note that an AE6 index of 250 nT corresponds to a Kp value of approximately 3_0.
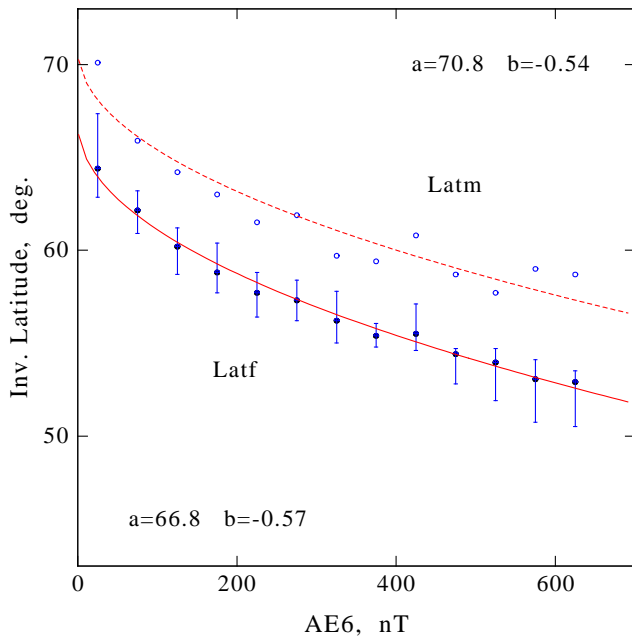
In order to illustrate the kind of correlation that exists between the AE6 index and the location of the polar cliff, all latf values were sorted into 50 nT-wide intervals of this index. For each of these intervals, the median and the upper and lower quartiles of the latf values were determined. They are indicated by the blue dots and bars in Fig. 3. As is evident, a fairly tight if non-linear correlation exists between both quantities. A simple function of the type

$$latf = a + b\sqrt{AE6} \tag{2}$$

does provide a good description of this correlation; see the solid red line. The associated coefficients are given in the lower left-hand corner. According to these data, the equatorward boundary of the polar cliff is located below 55° invariant latitude during storm conditions.

A similar correlation study was also performed on the latitude of the poleward boundary of the density rise, i.e., on latm. The results obtained in this case are indicated by the medians (open blue circles) and the dashed red regression line. The line parameters are given in the upper right-hand corner. As can be seen, both boundaries of the polar cliff move at about the same rate towards lower latitudes with increasing geomagnetic activity. Their mean distance is about 4°. For the Kp index, the correlation is less tight (the mean interquartile ranges are 3.6 and 2.6, respectively) but linear; see Fig. 14.

Besides depending on geomagnetic activity, the location of the polar cliff varies also with geographic longitude. In order to isolate this relatively small variation, we first removed the much larger changes with geomagnetic activity. To this end

Fig. 3. Location of the polar cliff as a function of geomagnetic activity. The AE6 index is indicated on the abscissa, the associated invariant latitudes of the equatorward (latf) and poleward (latm) boundaries of the polar cliff on the ordinate. The median and the upper and lower quartiles of these latter parameters were determined for each 50 nT-wide interval of the AE6 index. In case of latf, these are indicated by the blue dots and bars. In case of latm, only the respective medians are shown (open blue circles). In both cases, the interquartile ranges are of the same order of magnitude (the mean interquartile ranges are 2.6° for latf and 3.7° for latm). Regression lines of the type latf, $m = a + b\sqrt{AE6}$ were fitted to the median values (latf: solid red line; latm: dashed red line). The associated coefficients are given in the lower left-hand (latf) and upper right-hand (latm) corners, respectively. Note that only few data points are available for AE6 values larger than, say, 600 nT; furthermore, that each median point has been given equal weight in the regression analysis; and finally, that a small part of the scatter is due to embedded variations with longitude and local time.
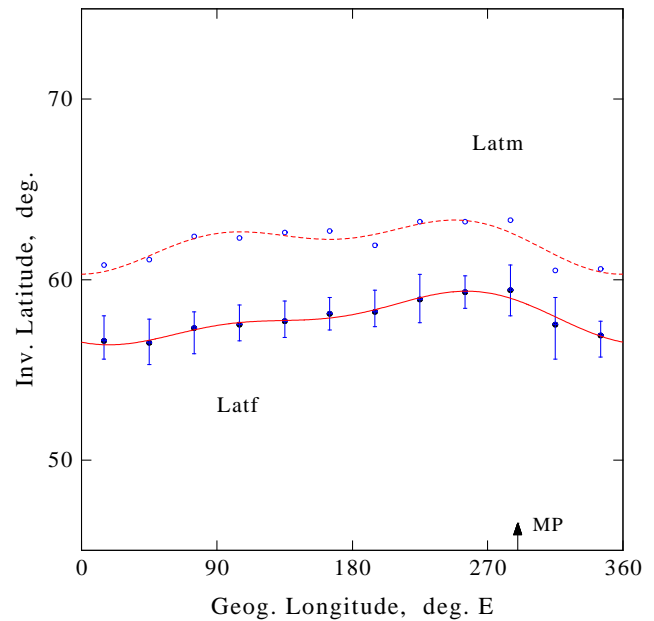
all latf and latm values were adjusted to a common level of geomagnetic activity (in our case $AE6_{ref} = 250$ nT)

$$\text{lat}_{adj} = \text{lat}_{obs} + (\text{lat}_{model}(AE6 = 250\,\text{nT})$$
$$-\text{lat}_{model}(AE6_{obs}))\,. \qquad (3)$$

Here lat_{model} is calculated using Eq. (2). After this adjustment, all latf and latm values were sorted into 30°-wide intervals of longitude. Their medians and quartiles are shown in Fig. 4. The format of data presentation corresponds to that in Fig. 3, except that this time sin and cos functions have been fitted to the data:

$$\text{latf, latm} = a_0 + a_1 \sin\Lambda + b_1 \cos\Lambda$$
$$+a_2 \sin(2\Lambda) + b_2 \cos(2\Lambda) \qquad (4)$$

with Λ = geographic longitude east in degrees, and the following sets of coefficients (57.8, −0.904, −0.761, −0.0083,

Fig. 4. Location of the polar cliff as function of geographic longitude. The format of data presentation corresponds to that in Fig. 3, except that this time a combination of sin and cos functions has been fitted to the median values. The analytic form of these regression lines is given in Eq. (4). An arrow indicates the position of the geomagnetic pole (MP). Note that the results presented in this figure refer to a geomagnetic activity level of AE6 = 250 nT; see text for details.

−0.534) for latf, and (62.0, −0.247, −1.002, 0.150, −0.751) for latm. As can be seen, the longitudinal variation is relatively small as compared to that with geomagnetic activity, and peak-to-peak changes are less than 3°. Note that the largest poleward shifts are observed in the neighborhood of the geomagnetic pole.
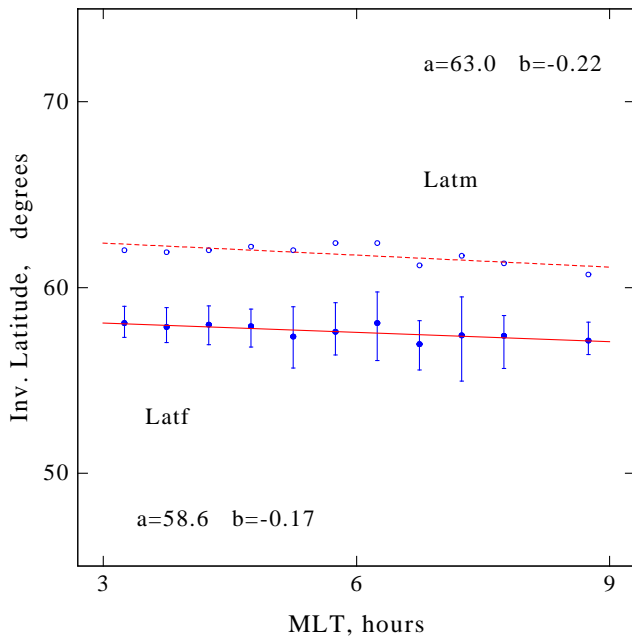
Of course, we also checked whether the location of the polar cliff depends on local time; see Fig. 5. As can be seen, there are hardly any changes with this parameter. In fact, for the local time range considered in this study, the total displacement amounts to less than 1.5°. Displacements of similar magnitude are observed for variations with altitude (not shown).

4　Magnitude of the density rise in the polar cliff

Besides the location, the magnitude of the density increase is of interest. Here the ratio of the densities observed at the pole- and equatorward boundaries of the polar cliff serves as a suitable measure of this quantity:

$$\text{relative density increase} = \frac{\text{Ne(latm)}}{\text{Ne(latf)}} = \frac{\text{Nem}}{\text{Nef}}. \qquad (5)$$

According to our data set, the median and the lower and upper quartiles of this relative density increase are 4.0, 2.8, and

Fig. 5. Location of the polar cliff as function of magnetic local time. The format of data presentation corresponds to that in Fig. 4, except that this time linear regression lines have been fitted to the median values. Again, the results refer to a geomagnetic activity level of AE6 = 250 nT.
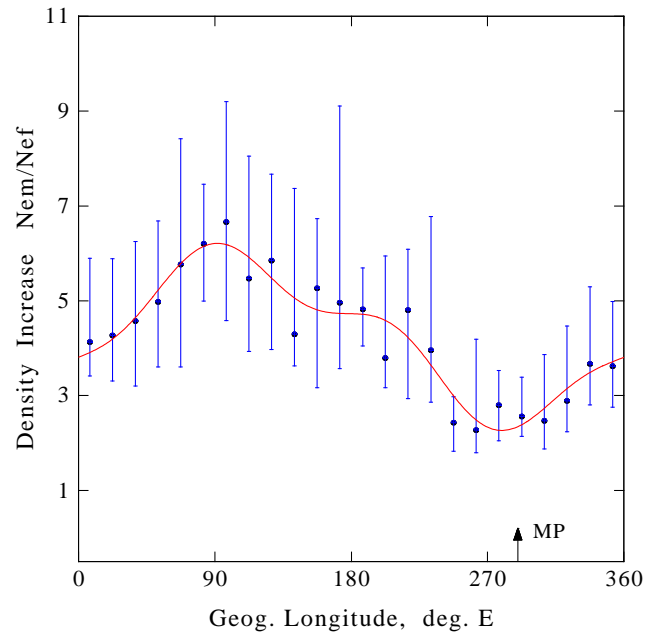

Fig. 6. Relative density increase in the polar cliff as function of geographic longitude. The geographic longitude is indicated on the abscissa, the relative density increase on the ordinate. The median (blue dots) and the upper and lower quartiles (blue bars) of this latter parameter were determined for each 15°-wide interval of the geographic longitude. A combination of sin and cos functions was fitted to the median values (solid red line; see Eq. 7). The location of the geomagnetic pole is indicated by an arrow. Note that the results presented in this figure refer to an altitude of 400 km; see text for details.

6.1, respectively. However, at times much larger values are observed (see, e.g., Fig. 12), and in 8 % of all cases it exceeds a factor of 10.

As to systematic variations, the magnitude of the density increase depends primarily on longitude and altitude. In order to document the changes with longitude, all density ratios were first adjusted to a common altitude of 400 km:

$$(\text{Nem/Nef})^{400\,\text{km}}_{\text{adj}} = (\text{Nem/Nef})^{h}_{\text{obs}} \cdot \left(\frac{(\text{Nem/Nef})^{400\,\text{km}}_{\text{model}}}{(\text{Nem/Nef})^{h}_{\text{model}}} \right). \quad (6)$$

Here the model values of the density ratio are calculated using Eq. (8). This adjustment somewhat reduces the considerable scatter of the data. Subsequently, all density ratios were sorted into 15°-wide intervals of geographic longitude. For each of these intervals, the median and the upper and lower quartiles were determined. This procedure leads to the longitudinal variation of the relative density increase as documented in Fig. 6. Most prominent is the increase of the density ratio near 90° E, and the pronounced minimum near 270° E, i.e., in the neighborhood of the geomagnetic pole. Again, a combination of sin and cos functions is used to describe these variations analytically:

relative density increase$(\Lambda, 400\,\text{km}) =$

$4.27 + 1.55 \sin \Lambda - 0.47 \cos \Lambda + 0.17 \sin(2\Lambda)$

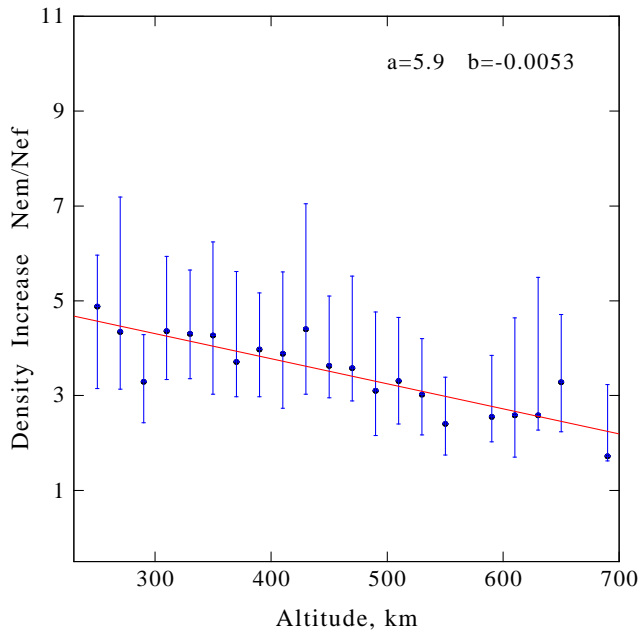$-0.002 \cos(2\Lambda) - 0.39 \sin(3\Lambda) + 0.007 \cos(3\Lambda).$ (7)

Here the longitude Λ is in degrees east. This approximation is indicated by the red curve in Fig. 6.

Likewise, the altitude dependence of the density increase was determined. First, all density ratios were adjusted to a common longitude of 0°. Next, they were sorted into 20 km-wide altitude intervals. For each of these intervals, the median and the upper and lower quartiles of the density ratios were determined. They are indicated by the blue dots and bars in Fig. 7. In spite of the considerable scatter of the data, there is a clear trend for the magnitude of the density rise to decrease with increasing altitude. This trend is reasonably well described by the linear regression line:

relative density increase$(h, 0°\,\text{E}) = 5.9 - 0.0053h.$ (8)

Here the altitude h is in kilometers. This approximation is indicated by the red line in Fig. 7.

What may come as a surprise is that the density increase depends only weakly on the level of geomagnetic activity; see Fig. 8. In fact, if the two median points immediately below and above 600 nT are neglected (the number of data points in these intervals is relatively small), the regression line would become horizontal, indicating no dependence on geomagnetic activity at all.
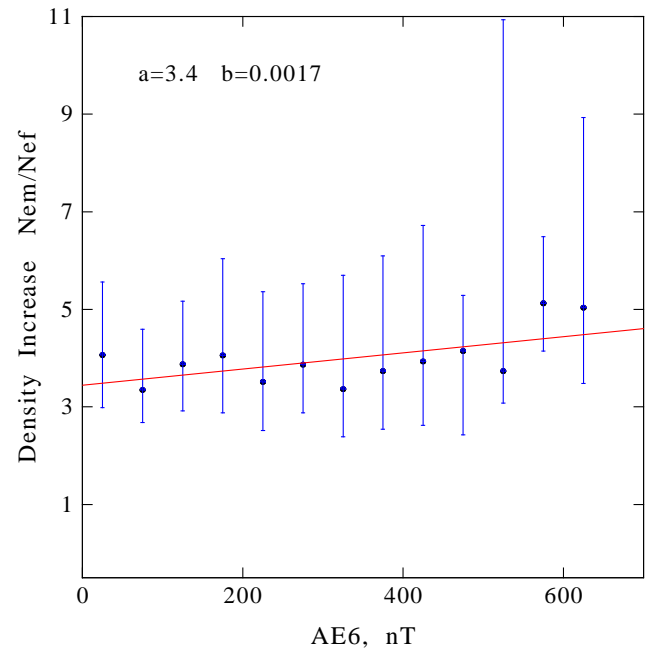
Fig. 7. Relative density increase in the polar cliff as function of altitude. The format of data presentation corresponds to that in Fig. 6, except that this time a linear regression line has been fitted to the data; the associated coefficients are given in the upper right-hand corner. Note that the results presented in this figure refer to a geographic longitude of 0°.
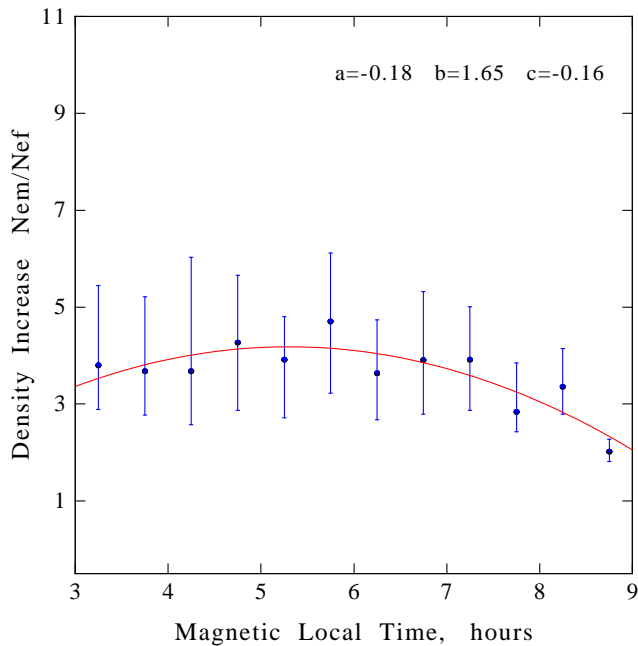

Fig. 8. Relative density increase in the polar cliff as function of geomagnetic activity. The format of data presentation corresponds to that in Fig. 7, except that the altitude is replaced by the AE6 index. Note that the data refer to a geographic longitude of 0° and an altitude of 400 km.

We also checked whether the density increase depends on local time; see Fig. 9. Again, no major changes are observed. For completeness sake, a second-order polynomial was fitted to the data and is shown by the red line in Fig. 9. The associated coefficients are given in the upper part of this figure.

5   Mean latitudinal profiles of the polar cliff and the associated temperature changes

Calculating the mean latitudinal profile of the polar cliff requires special care. This is because the density rise is confined to a relatively narrow latitudinal range whose position is constantly changing, primarily with the level of geomagnetic activity. Therefore, simply averaging the individual profiles would invariably smear out the density increase. To avoid this kind of distortion, a superposed epoch type of averaging procedure was used in the present study.

In a first step, all density values of a latitudinal profile were normalized. This facilitates a comparison of density profiles obtained during different geophysical conditions. Here the density value Nef measured at the foot of the polar cliff serves as a suitable normalization standard. Next, all latitudinal profiles were superimposed in such a way that the foot points latf were aligned and located at a common reference location (i.e., latf ⇒ latref = 0). This way the basic latitudinal structure of the density increase is preserved when averaging

the data. Subsequently, spline functions were fitted to each profile. This allowed us to calculate the densities at 1° steps relative to the new reference location. Subsequently, the median and the upper and lower quartiles of the density values were determined for each degree of this new coordinate system. Finally, spline functions were fitted to these parameters. The end product of this procedure is presented in Fig. 10.

As indicated by the shaded area between the lower and upper quartiles, the scatter of the data is quite substantial. It is partly due to the different height ranges covered by each profile, and also to differences in the geophysical conditions. Nevertheless, the mean electron density rise in the polar cliff stands out as a relatively narrow feature, not unlike those actually observed. Note that the latitudes indicated on the abscissa refer to an AE6 index of 250 nT. For this level of geomagnetic activity, the beginning of the density increase is located near 58° invariant latitude; see Eq. (2). For other conditions, the mean profile has to be shifted towards higher or lower latitudes, depending on whether the geomagnetic activity considered is lower or higher.

How does the electron temperature behave in the neighborhood of the polar cliff? To answer this question, mean latitudinal profiles of the electron temperature were generated, again using the latitude of the foot of the polar cliff latf as a common reference location. The result is presented in Fig. 11. As can be seen, the electron temperature exhibits a fairly sharp drop within the polar cliff. Evidently – and

Fig. 9. Relative density increase in the polar cliff as function of magnetic local time. The format of data presentation corresponds to that in Fig. 6, except that this time a polynomial of the form $a + b \cdot \text{MLT} + c \cdot \text{MLT}^2$ has been fitted to the median values. Again, the data refer to a geographic longitude of $0°$, and an altitude of 400 km.

Fig. 10. Mean latitudinal profile of the polar cliff. The median of 610 density profiles is plotted (red curve). These profiles have been superimposed in such a way that the latitude of the foot of the polar cliff latf serves as a common reference location. In addition, all density values of a profile have been normalized to the respective density value Nef observed at this location. The blue-shaded area indicates the range between the upper and lower quartiles. The latitudes given on the abscissa apply to a geomagnetic activity level of AE6 = 250 nT. For other activity conditions the mean profile should be shifted to higher or lower latitudes, in accord with the results presented in Fig. 3 and Eq. (2).

in agreement with previous findings – there is a clear anti-correlation between changes in the electron density and electron temperature, at least on average. Looking at individual data sets, things often become more complicated and different effects may modify this strict anti-correlation.
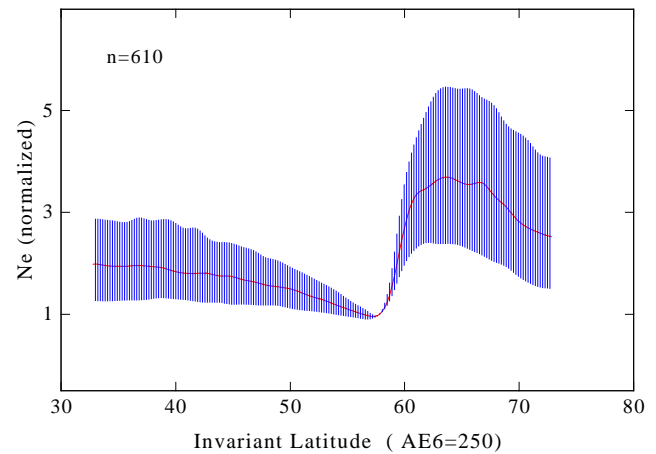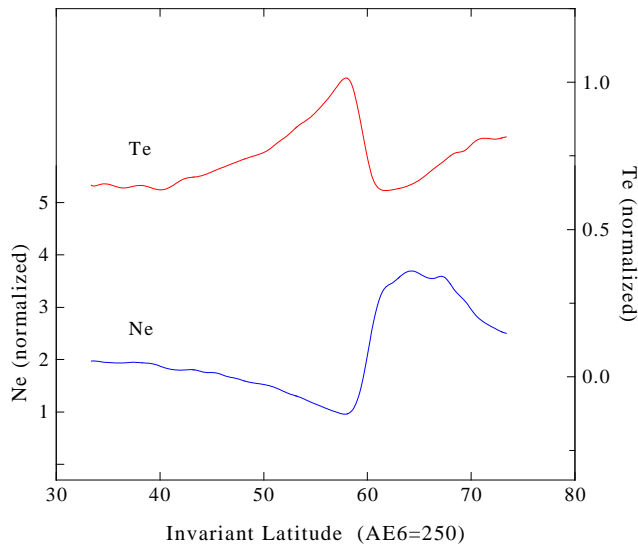
6 Discussion

In the preceding sections, the mean properties of the polar cliff were determined. Here they are discussed and compared to related observations. First, an attempt is made to explain the systematic variations. Next, it is argued that in the morning sector the polar cliff is not part of an ionospheric trough. Finally, we briefly comment on the origin of the polar cliff.

6.1 Systematic variations

As documented in Fig. 4, the position of the polar cliff strongly depends on the level of geomagnetic activity. This certainly does not come as a surprise, since all magnetospherically controlled phenomena exhibit this behavior: they all move towards lower latitudes with increasing geomagnetic activity. In fact, even the rate at which this occurs is of comparable magnitude; see, for example, Fig. 14.

What does come as a surprise, however, are the pronounced changes of the polar cliff properties with geographic

longitude. How can we explain these remarkable variations? Here it is suggested that they are not so much an intrinsic characteristic of the polar cliff itself. Instead they are induced – at least partly – by asymmetries in the longitudinal distribution of the ionization density at middle latitudes. This is illustrated in Fig. 12. Here we compare two density profiles, one recorded near the longitude of the geomagnetic pole, the other one 122° apart from it. All other geophysical conditions are almost the same. As can be seen, the background ionization density at middle latitudes is significantly higher near the longitude of the geomagnetic pole. Accordingly, the density increase in the polar cliff is significantly reduced at this location. Also, the foot of the polar cliff is slightly displaced towards higher latitudes, in agreement with our statistical results. The lower panel in Fig. 12 illustrates that the density anomaly at middle latitudes may be so pronounced that it severely distorts the density profile in the neighborhood of the polar cliff.

In this context, it should be remembered that comparable longitudinal variations are also observed for the subauroral ionospheric trough in the evening sector (e.g., Karpachev et al., 1996; Prölss, 2007). In that case, the height of the equatorward wall of the trough is largest near the geomagnetic pole.

As to the altitude dependence of the density increase in the polar cliff, Fig. 11 provides a plausible explanation. Since the electron temperature is significantly reduced within the polar cliff region, this applies also to the density scale height.
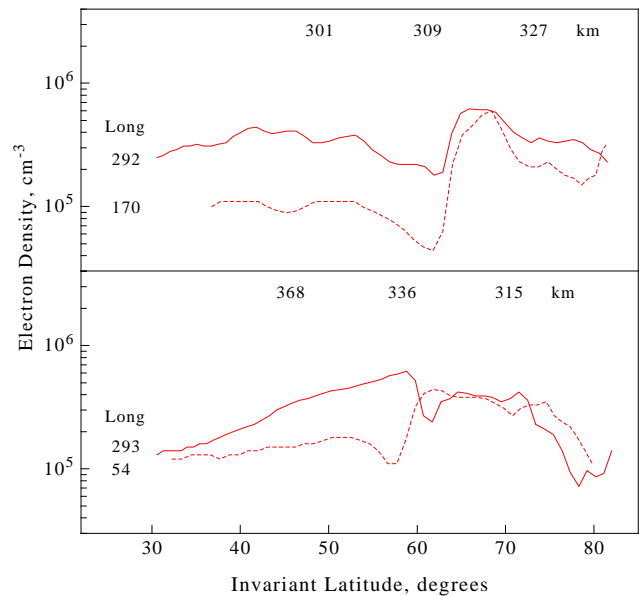
Fig. 11. Mean latitudinal profiles of the electron density (blue curve) and electron temperature (red curve) at the location of the polar cliff. The format of data presentation corresponds to that in Fig. 10, except that this time only the median curves are shown. In both cases, the foot of the polar cliff latf serves as a common reference location. In addition, all density and temperature values have been normalized to the respective density and temperature values Ne (latf) and Te (latf) observed at this location.

Therefore, within the polar cliff, the electron density will decrease more rapidly with altitude than equatorward of this region. This in turn leads to a reduction of density differences and therefore to a decrease of the density rise in the polar cliff with altitude.

6.2 Polar cliff and ionospheric trough

Should the polar cliff be considered as part of an ionospheric trough? For the evening sector, this question should certainly be answered in the affirmative. In the morning sector, however, things are different, and this is documented in Fig. 13. Compared are two mean density profiles. The upper one refers to the polar cliff in the morning sector (see Fig. 10); the lower one to the ionospheric trough in the evening sector. Evidently, there are significant differences. In the morning sector, the ionization density gradually decreases with increasing latitude. This smooth decline is interrupted by a sudden rise in the ionization density in the polar cliff. By necessity, a minimum forms where these opposite trends meet. In the evening sector, we also observe initially a gradual decrease of the ionization density. This time, however, the smooth decline is interrupted not by a sudden rise but by a sudden drop of the ionization density. And a minimum forms where this steep drop ends and a moderate recovery sets in. It is this partial recovery that forms the polar wall of the ionospheric trough.
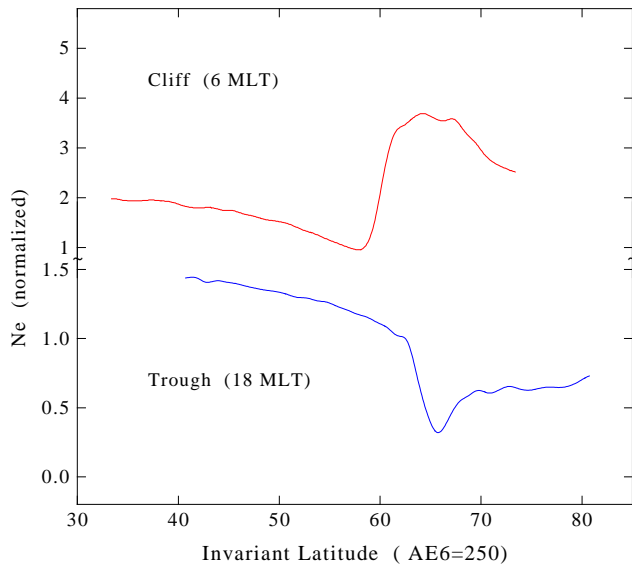

Fig. 12. Comparison of electron density profiles observed in different longitude sectors. In both cases, one profile was recorded near the longitude of the geomagnetic pole (solid red line), the other one about 120° apart (dashed red line). The format of data presentation corresponds to that in Fig. 1, except that this time the geographic longitudes, not the universal times, are indicated. The measurements presented in the upper panel were obtained on 23 December 1981; they refer to about 06:00 MLT and low levels of geomagnetic activity (Kp ≤ 2₊) throughout the period of interest. Similar conditions apply to the data set collected on 14 December 1981, which is presented in the lower panel.

In the literature, both density profiles are often classified as trough structures (e.g., Werner and Prölss, 1997; Karpachev, 2003). However, this only becomes possible if the initially very restrictive definition of a trough (e.g., Mendillo and Chacko, 1977) is considerably relaxed. Here we prefer not to follow this convention. We believe that the steep density drop in the equatorward wall is an essential and defining feature of an ionospheric trough. And, this density drop is not observed in the morning sector. Therefore we believe that the subauroral ionospheric trough does not extend into this local time sector. This also implies, of course, that in the morning sector the polar cliff is not part of this phenomenon.

6.3 Origin of the polar cliff

As to the origin of the polar cliff, direct auroral particle precipitation has long been suspected to be responsible for this phenomenon. At least in the morning sector, this explanation is clearly insufficient. In Fig. 14, we compare the equatorward boundaries of the polar cliff (latf) and diffuse auroral electron precipitation (Epb; Gussenhoven et al., 1981). Whereas there is excellent agreement as to the slopes of both regression lines, it is clear that the electron precipitation
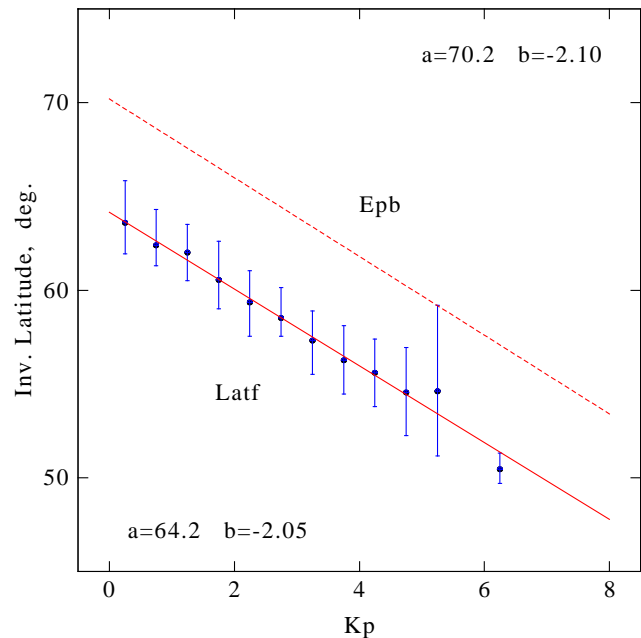
Fig. 13. Mean electron density profiles as obtained for two different local time sectors. The upper red curve refers to the morning sector and represents the mean polar cliff profile given in Fig. 10. The lower blue curve refers to the evening sector and represents the mean trough profile derived in (Prölss, 2007).

occurs at much higher latitudes. This is consistent with results presented by Rodger et al. (1986; see their Figs. 1c and 2). The same kind of displacement should apply for auroral ion precipitation (e.g., Gussenhoven et al., 1987; Hardy et al., 1989). We are therefore left with soft particle precipitation from the inner magnetosphere. Soft particle precipitation, because the more energetic ring current particles deposit their energy below the F region peak (e.g., Schröder and Prölss, 1991; Fang et al., 2007). That soft particle precipitation from the inner magnetosphere is sufficient to support the polar cliff in the morning sector has yet to be demonstrated.

An alternate – and more appealing – explanation of the polar cliff is based on the transport of ionization (e.g., Rodger et al., 1986; Rodger, 2008; Middleton et al., 2008). As suggested by these authors, the higher density plasma in the polar cliff is originally produced by solar radiation in the daytime sector. Subsequently, it is convected by electric fields over the polar cap to the nightside and around towards dawn in a tongue-of-ionization. Simulations performed with the coupled thermosphere–ionosphere–plasmasphere model support this explanation. It would also be consistent with our observation that the density increase depends only weakly on the level of geomagnetic activity.

Fig. 14. Equatorward boundaries of the diffuse auroral electron precipitation (Epb) and polar cliff (latf) as function of geomagnetic activity. The auroral precipitation data are taken from (Gussenhoven et al., 1981). Since these authors use the Kp index to describe the level of geomagnetic activity, our data were replotted accordingly.

7   Summary

This study investigates a phenomenon that we called "polar cliff". It consists of a steep density increase in the morning sector of the polar ionosphere. For the Northern Hemisphere winter, the mean properties of this remarkable feature may be summarized as follows.

– During moderate geomagnetic activity, the foot of the polar cliff is located below 60° invariant latitude. Here, within about 4°, the ionization density increases by a factor of 4, on average.

– The location of the polar wall depends primarily on the level of geomagnetic activity. Other variations like those with longitude, and especially those with local time and altitude, are of secondary importance. The rate at which the polar wall moves equatorward with increasing geomagnetic activity is of the order of 1.5° per 100 nT increase in the AE6 index, and 2° per increase of the Kp index by 1.

– The magnitude of the density rise depends primarily on longitude and altitude. Other variations, like those with geomagnetic activity and local time are barely significant. As to the variation with altitude, the magnitude of the density rise decreases linearly by a factor of 0.6 per 100 km altitude increase. The longitudinal variations are

more complex, with the smallest density increases observed near the geomagnetic pole.

– Within the polar cliff, the electron temperature exhibits a significant decrease. This may explain why the magnitude of the density rise decreases with increasing altitude.

– The most surprising variations are those with geographic longitude. Here they are attributed to asymmetries in the background ionization density at middle latitudes.

– It is also argued that the subauroral ionospheric trough does not extend into the morning sector. Therefore the polar cliff is not considered part of this phenomenon.

– As to the origin of the polar cliff, local auroral particle precipitation should be less important, at least in the morning sector. Transport of ionization is an alternate and very appealing explanation for this fascinating phenomenon.

References

Andrews, M. and Thomas, J.: Electron density distribution above the winter pole, Nature, 221, 223–227, 1969.

Dudeney, J., Rodger, A., and Jarvis, M.: Radio studies of the main F region trough in Antarctica, Radio Sci., 18, 927–936, 1983.

Fang, X., Liemohn, M., Kozyra, J., and Evans, D.: Global 30–240 keV proton precipitation in the 17–18 April 2002 geomagnetic storms: 2. Conductances and beam spreading, J. Geophys. Res., 112, A05302, doi:10.1029/2006JA012113, 2007.

Gussenhoven, M., Hardy, D., and Burke, W.: DMSP/F2 electron observations of equatorward auroral boundaries and their relationship to magnetospheric electric fields, J. Geophys. Res., 86, 768–778, 1981.

Gussenhoven, M., Hardy, D., and Heinemann, N.: The equatorward boundary of auroral ion precipitation, J. Geophys. Res., 92, 3273–3283, 1987.

Hardy, D., Gussenhoven, M., and Brautigam, D.: A statistical model of auroral ion precipitation, J. Geophys. Res., 94, 370–392, 1989.

Hoffman, R. and Schmerling, E.: Dynamics Explorer program: An overview, Space Sci. Instr., 5, 345–348, 1981.

Karpachev, A.: The dependence of the main ionospheric trough shape on longitude, altitude, season, local time, and solar and magnetic activity, Geomag. Aeron., 43, 239–251, 2003.

Karpachev, A., Deminov, M., and Afonin, V.: Model of the mid-latitude ionospheric trough on the base of Cosmos-900 and Intercosmos-19 satellites data, Adv. Space Res., 18, 221–230, 1996.

Krehbiel, J., Brace, L., Theis, R., Pinkus, W., and Kaplan, R.: The Dynamics Explorer Langmuir probe instrument, Space Sci. Instr., 5, 493–502, 1981.

Liszka, L.: Variation according to latitude of the electron content of the ionosphere near the auroral zone, Nature, 208, 280–281, 1965.

Mendillo, M. and Chacko, C.: The baselevel ionospheric trough, J. Geophys. Res., 82, 5129–5137, 1977.

Middleton, H., Pryse, S., Wood, A., and Balthazor, R.: The role of the tongue-of-ionization in the formation of the poleward wall of the main trough in the European post-midnight sector, J. Geophys. Res., 113, A02306, doi:10.1029/2007JA012631, 2008.

Prölss, G.: Electron temperature enhancement beneath the magnetospheric cusp, J. Geophys. Res., 111, A07304, doi:10.1029/2006JA011618, 2006a.

Prölss, G. W.: Subauroral electron temperature enhancement in the nighttime ionosphere, Ann. Geophys., 24, 1871–1885, doi:10.5194/angeo-24-1871-2006, 2006b.

Prölss, G. W.: The equatorward wall of the subauroral trough in the afternoon/evening sector, Ann. Geophys., 25, 645–659, doi:10.5194/angeo-25-645-2007, 2007.

Prölss, G.: Perturbations of the upper atmosphere in the cleft region, J. Atmos. Sol-Terr. Phys., 70, 2374–2380, 2008.

Rodger, A.: The mid-latitude trough – revisited, in: Midlatitude Ionospheric Dynamics and Disturbances, edited by: Kintner, P., Coster, A., Fuller-Rowell, T., Mannucci, A., Mendillo, M., and Heelis, R., Geophys. Monogr. Ser., Vol. 181, 25–33, 2008.

Rodger, A., Brace, L., Hoegy, W., and Winningham, J.: The poleward edge of the mid-latitude trough – its formation, orientation and dynamics, J. Atmos. Terr. Phys., 48, 715–728, 1986.

Schröder, S. and Prölss, G.: Heating of the upper atmosphere by oxygen ions precipitated from the ring current, Ann. Geophys., 9, 267–272, 1991,
http://www.ann-geophys.net/9/267/1991/.

Taylor, G.: Structure at the poleward edge of a mid-latitude F-region trough, J. Atmos. Terr. Phys., 35, 647–656, 1973.

Thomas, J., Rycroft, M., Colin, L., and Chan, K.: Experimental results from the Alouette I satellite, in: Electron density profiles in ionosphere and exosphere, edited by: Frihagen, J., 322–357, North-Holland Publ. Comp., Amsterdam, 1966.

Werner, S. and Prölss, G.: The position of the ionospheric trough as a function of local time and magnetic activity, Adv. Space Res., 20, 1717–1722, 1997.